Supporting Information for the Manuscript

An ultrastable porous metal-organic framework luminescent switch towards aromatic compounds

Fei-Yan Yi,[a] Ying Wang,[a] Jian-Ping Li,[a] Dai Wu,[a] Ya-Qian Lan,*[b] and Zhong-Ming Sun*[a]

[a]*State Key Laboratory of Rare Earth Resource Utilization, Changchun Institute of Applied Chemistry, Chinese Academy of Sciences, 5625 Renmin Street, Changchun, Jilin 130022, P. R. China. Tel: 86-431-85262389; Fax: 86-431-85698041*

[b]*School of Chemistry and Materials Science, Nanjing Normal University, Nanjing, Jiangsu 210023, P. R. China*

Email: szm@ciac.ac.cn; yqlan@njnu.edu.cn

Table of Contents

1. Experimental section

➢ Materials and Methods

H_6L was synthesized by a modified procedure documented previously.[1] All other reagents and solvents were obtained from commercial sources and used as received.

Elemental analyses for C, H and N in the solid sample were carried out on a VarioEL analyzer. The infrared (IR) spectra (diamond) were recorded on a Nicolet 7600 FT-IR spectrometer within the 4000-500 cm^{-1} region. TGA (thermal gravimetric analysis) was recorded under an air atmosphere with a heating rate of 10 °C/min using a a SDT 2960 Simultaneous DSC-TGA of TA instrument in the temperature range of 50-800 °C. Powder X-ray power diffraction (PXRD) patterns were collected by a D8 Focus (Bruker) diffractometer with Cu Kα radiation Field-emission (λ = 0.15405 nm). The gas adsorption isotherms for N_2 at 77 K, H_2 at 77 K and 87 K, CO_2 at 273 K and 298 K were performed on ASAP 2050 V1.01 E and Autosorb MP-1 apparatuses at 1 atm. The vapor adsorption isotherm for benzene at 293 K was performed on an Autosorb iQ Station 2 apparatuses of Quantachrome Instrument (version 3.01).
A basic trinuclear cluster-model $[Cd_3(bipy)_2(L)]$ was constructed according to the experimental data. All the calculations for the studied complexes were performed with *C*1 symmetry using the Gaussian 09 package[2]. B3LYP[3] together with the 6-31G basis set for C, H, N, O atoms and the LANL2DZ basis set for the Cd element were chosen for the structure optimization. Time dependent DFT (TD-DFT)[4-6] calculations were performed on the basis of the optimized ground equilibrium geometries. The polarized continuum model (PCM)[7-9] in water, benzene, and Nitro-benzene was considered. GaussSum 2.5[10] was used for orbitals and the DOS analysis for structures and orbital manipulations.

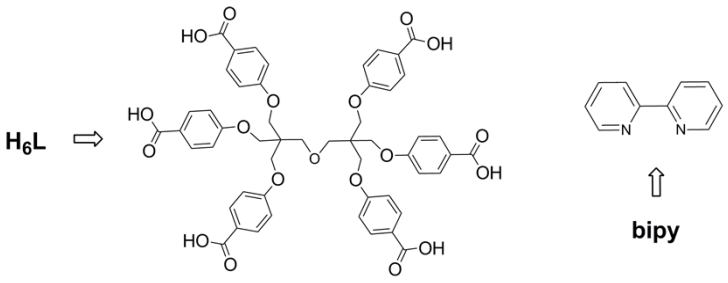

Scheme S1. Schematic representation of ligands H_6L and bipy.

➢ X-ray crystal structure determination:

Diffraction intensity data for single crystal of **1** was collected at 273 K on a Bruker Apex II CCD diffractometer equipped with graphite-monochromated Mo-Kα radiation (λ = 0.71073 Å). Data processing was accomplished with the SAINT program. Absorption corrections were applied using SADABS.[11] The structure was solved by direct methods using SHELXS-97 program of the SHELXTL package and refined by using the full-matrix least squares method on F^2 with SHELXTL-97.[12] Anisotropic displacement parameters were applied to all non-hydrogen atoms. Hydrogen atoms were located geometrically and were added to the structure factor calculation. The remained solvent molecules in the channels of **1** were disordered and could not be modeled properly, and the contribution of their electron density

was removed by the SQUEEZE routine in PLATON, which was determined by elemental analysis and thermogravimetric analysis. The formula for **1** was also determined by combining single-crystal structure, elemental microanalysis and TGA. A summary of the crystallographic data for complex **1** is listed in Table S1. CCDC-1017377 contains the supplementary crystallographic data for this paper. This data can be obtained free of charge from The Cambridge Crystallographic Data Centre via www.ccdc.cam.ac.uk/data_request/cif.

Table S1. Summary of Crystal Data and Structure Results for **1**.

Compound	1
chemical formula	$C_{88}H_{92}Cd_3N_8O_{23}$
structural formula	$\{Cd_3(L)(bipy)_2\bullet 4DMA\}_n$
fw	1966.90
temperature (K)	273(2)
a (Å)	31.136(9)
b (Å)	20.048(6)
c (Å)	15.849(4)
α (°)	90
β (°)	108.347(5)
γ (°)	90
V (Å^3)	9390(4)
Z	4
space group	*C*2/c
2θ max (deg)	50.34
μ(Mo-Kα) mm^{-1}	0.746
D (g/cm^3)	1.391
F(000)	4016
Reflections collected / unique	23749/8371 [R_{int} = 0.0792]
R_1[a] wR_2[b] [$I > 2\sigma(I)$]	R_1 = 0.0841, wR_2 = 0.2592
R_1[a] wR_2[b] (all data)	R_1 = 0.1211, wR_2 = 0.2854
GOF	1.011

[a] $R_1 = \sum||F_o| - |F_c||/\sum|F_o|$, [b] $wR_2 = \{\sum w[(F_o)^2-(F_c)^2]^2/\sum w[(F_o)^2]^2\}^{1/2}$

2. Structural figures

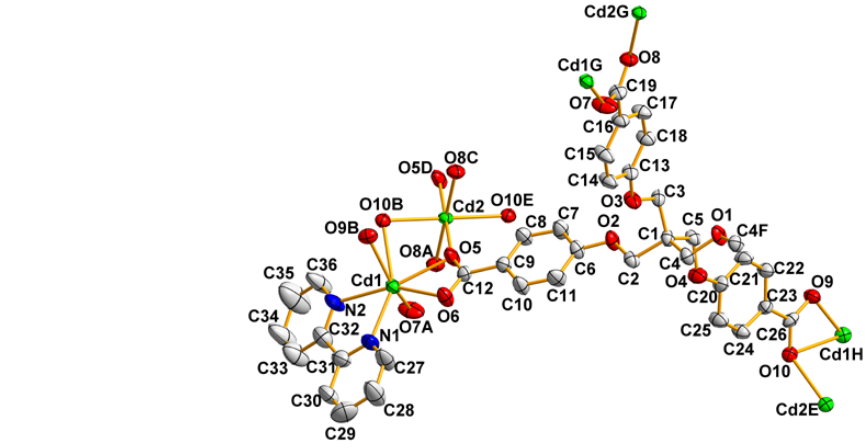

(a)

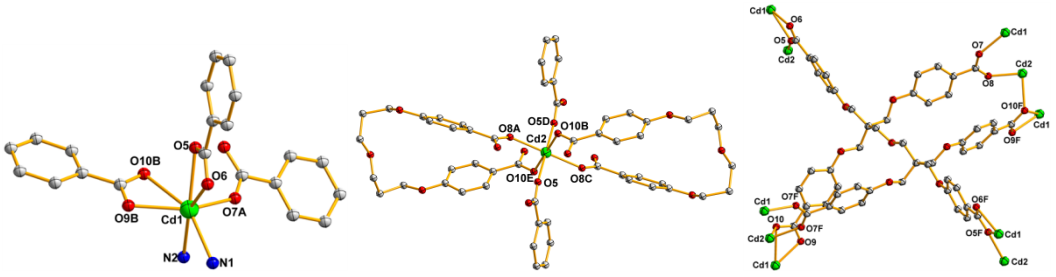

(b) (c) (d)

Fig. S1 (a) An ORTEP representation of the asymmetric unit of **1**. Thermal ellipsoids are drawn at the 30% probability level. The hydrogen atoms and free solvent molecules are omitted for clarity. Symmetry codes: A x, y, z-1; B x-1/2, -y+1/2, z-1/2; C -x+1/2, -y+1/2, -z+1; D -x+1/2, -y+1/2, -z; E -x+1, y, -z+1/2; F -x+1, y, -z+3/2; G x, y, z+1; H x+1/2, -y+1/2, z+1/2. (b-d) The coordination modes of Cd(1) (b), Cd(2) (c) and carboxylate ligand (d).

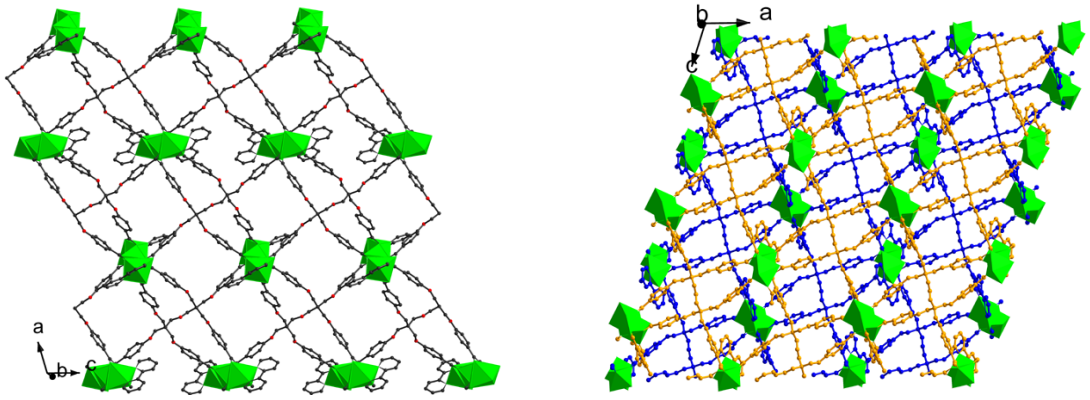

(a) (b)

Fig. S2 (a) A 2D layered structure in **1** along [010] direction. Color modes: carbon, gray; oxygen, red. The CdO_xN_y (x = 5, y = 2 for Cd(1); x = 6, y = 0 for Cd(2)) polyhedra are shaded in green. (b) Each double-layer in **1** is drawn in gold and blue, respectively.

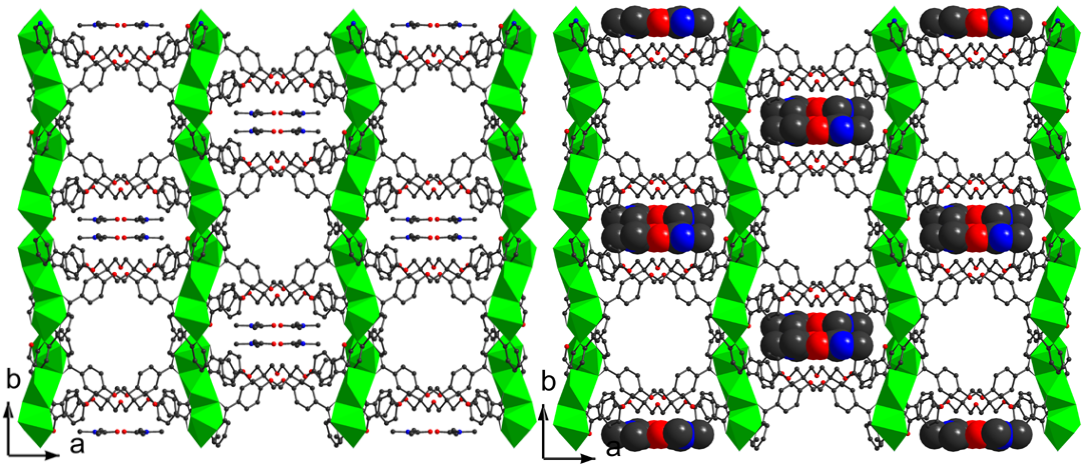

Fig. S3 View of the 3D supramolecular structure for **1** along *c*-axis, in which free DMA molecules filled into the 1D channels.

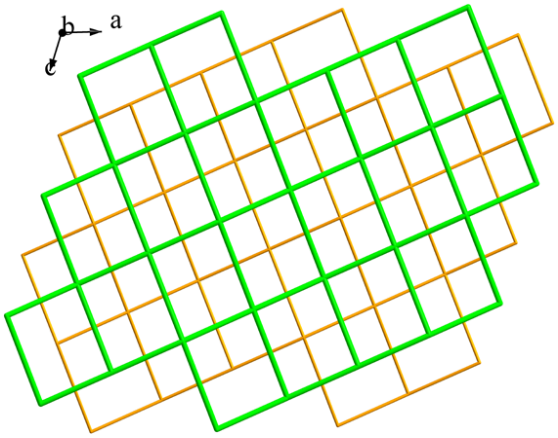

Fig. S4 The simplified (4, 4)-connected **sql** double-net shown in green and gold sticks, respectively.

3. TGA, PXRD and IR

3.1 TGA analyses

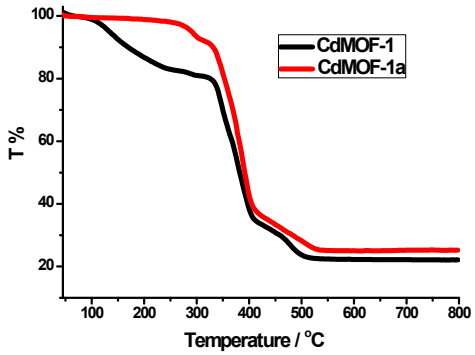

Fig. S5 TGA curves of CdMOF (**1**) and activated **1a** under air atmosphere.

As shown in Fig. S5-black line, the TG curve for **1** shows that the first weight loss of 17.3% from 86 °C to 258 °C correspond to the losses of four DMA molecules (cald. 17.7%). Then two

continuous weight losses in the temperature range of 316-518 °C corresponds to the combustion of organic ligands, implying that the complex decomposes. A plateau of 22.2% at 518 °C is observed. The final residual for Cd-MOF (**1**) was not characterized due to the its corrosive reactions with the TGA buckets made of Al_2O_3, however it is expected to be mainly cadmium(II) oxide.

Activated sample **1a** was also tested its thermal stability based on TGA curve (Fig. S5-red line). It can be seen clearly that **1** can completely release its guest molecules to form guest-free framework **1a**, and the solvent-free **1a** is highly stable until 265 °C. Considering the intrinsic structural property as well as combining its highly thermal stability and solvent-stability, it is anticipated that guest-free **1a** is a potential luminescent sensor for small solvent molecules at room temperature.

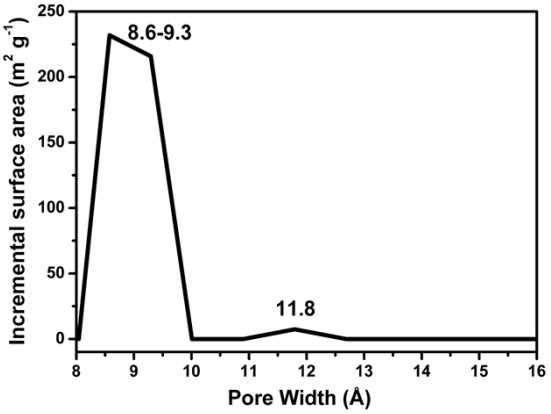

Fig. S6 Pore size distribution of **1a** based N_2 sorption data at 77 K.

3.2 PXRD analyses

As shown in Fig. S7, the diffraction peaks of the measured Cd-MOF (**1**) are almost in good agreement with the simulated data generated from the result of single-crystal diffraction data, confirming the phase purity of the as-synthesized samples.

Prior to the measurement of gas adsorption, some preparatory work has been done. The as-synthesized sample of **1** was immersed into anhydrous methanol for 3 days, methanol was refreshed three times during the exchange. Then similar immersion was utilized to treat the sample with dichloromethane to remove methanol molecules. After the removal of dichloromethane by centrifuging, the wet sample was dried under vacuum at 80 °C for 15 h to yield an activated **1** (denoted as **1a**). Its PXRD pattern, as depicted in Fig. S8 (**activated 1**), is almost identical to that of **1**, demonstrating the framework's robustness of activated **1a**.

Cd-MOF (**1**) and activated **1a** are insoluble in water and common organic solvents. Before the luminescent sensing study, the solvent-stabilities of **1a** treated by water and other different organic solvents (**1a/solvents**) are also demonstrated by PXRD (Fig. S8). The samples of **1a**/solvents were prepared by introducing each grinding sample (30 mg) into various solvents (N, N′-dimethylformamide (DMF), H_2O, benzene, nitrobenzene, 2-nitrotoluene, nitromethane, 2-propanol, acetonitrile, methanol, ethanol, tetrahydrofuran (THF), carbon tetrachloride (CCl_4)), and then aged for 72 h. Then the powder was obtained by filtration, and dried. As shown in Figure S8, it is clear that the basic frameworks of **1a** are still maintained after immersing solvent molecules, illustrating good solvent-stability.

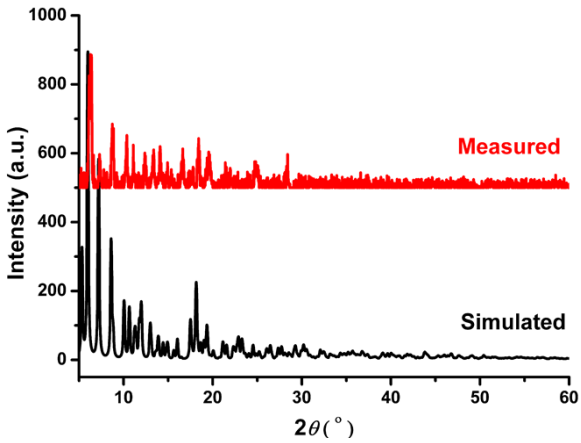

Fig. S7 The PXRD of as-synthesized sample **1** (red) and the calculated pattern (black) from the crystal structure of **1**.

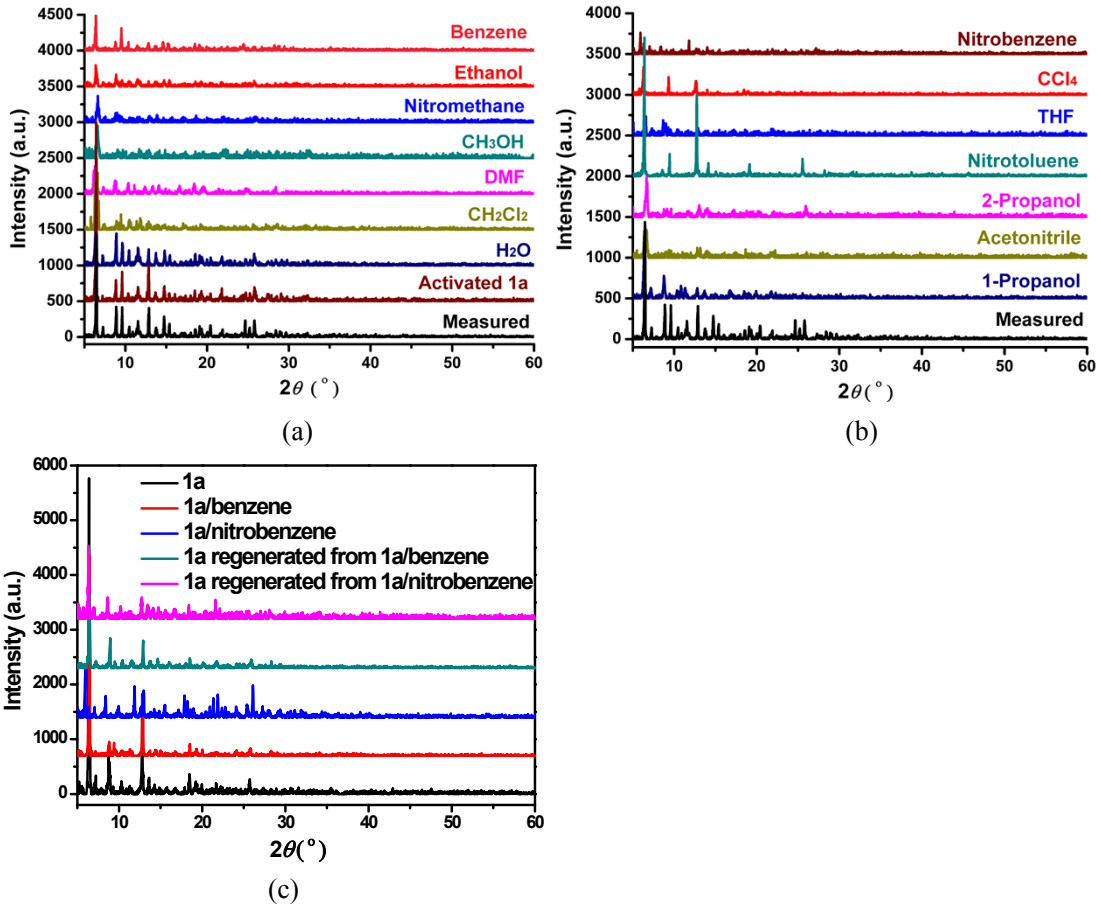

Fig. S8 PXRD patterns of **1a** (**activated 1**) and **1a** after immersed in various solvents (a and b), as well as **1a** regenerated from **1a**/benzene and **1a**/nitrobenzene (c).

3.3 FTIR analyses

IR peaks (cm^{-1}) for **1/benzene**: 3066 (w), 2927 (w), 2876 (w), 1672 (w), 1595 (s), 1522 (m), 1471 (w), 1435 (w), 1388 (vs), 1311 (m), 1244 (s), 1167 (m), 1106 (w), 1018 (m), 858 (m), 781 (m), 761 (m), 735 (w), 699 (w).

IR peaks (cm^{-1}) for **1/nitrobenzene**: 3071 (w), 2938 (w), 2881 (w), 1595 (s), 1517 (vs), 1471 (w),

1440 (w), 1388 (s), 1343 (s), 1311 (w), 1244 (m), 1167 (m), 1106 (w), 1018 (m), 848 (m), 781 (m), 756 (w), 735 (w), 699 (m).

As shown in Fig. S9b, some bands for Cd-MOF (**1**) are different from free H_6L and bipy ligands, due to the formation of Cd^{II}-O and Cd^{II}-N coordination bonds of carboxylate oxygen atoms and nitrogen atoms from H_6L and bipy ligands. The infrared spectra of various solvent-soaked **1 (1/solvents)** (Fig. S10) further confirm that the framework of **1/solvents** is retained after the introduction of organic solvents.

In the IR spectra of **1/benzene**, **1/nitrobenzene**, **1/DMF**, and **1/H_2O**, one adsorption band is abrupt and abnormal at about 2500 cm^{-1}, that should be attributed to the asymmetric vibration from free linear carbon dioxide (ν_{asym} = 2348 cm^{-1}) in air, found in the background spectrum (Fig. S9-**background**), which is caused by instrument.

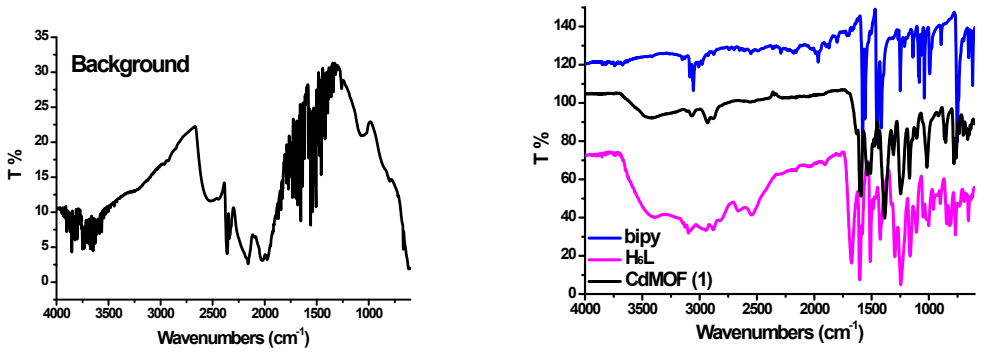

(a) (b)

Fig. S9 FTIR of free bipy, H_6L ligands and Cd-MOF (**1**).

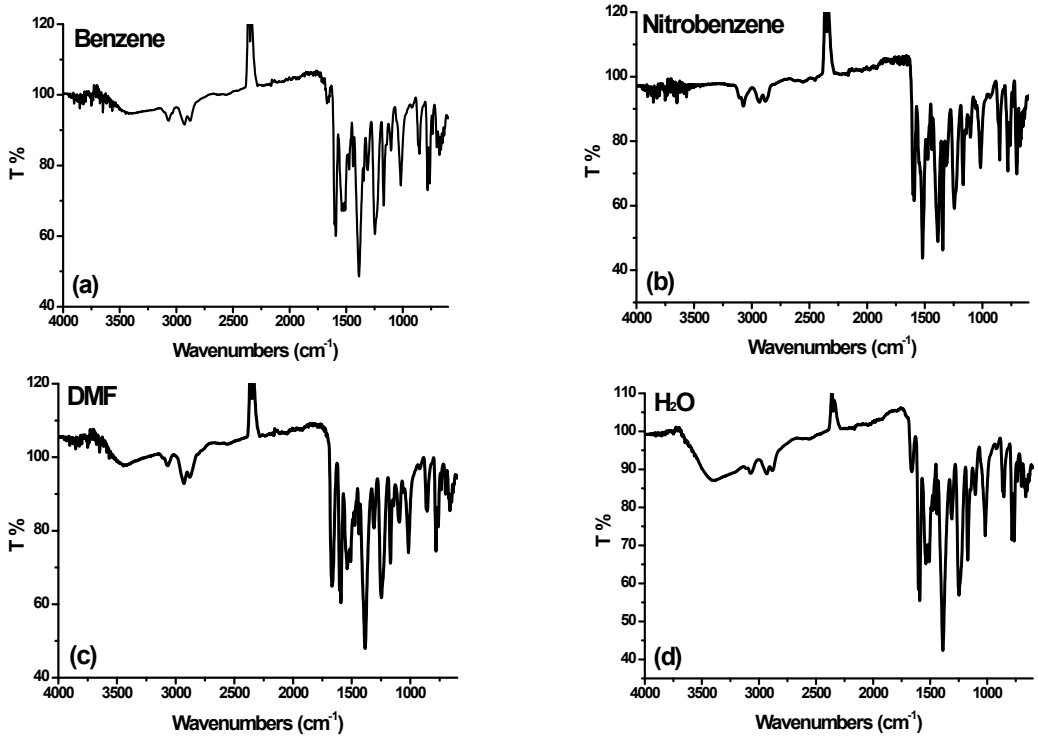

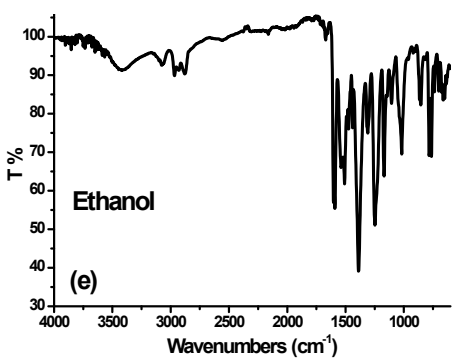
Ethanol
(e)
T %
Wavenumbers (cm-1)

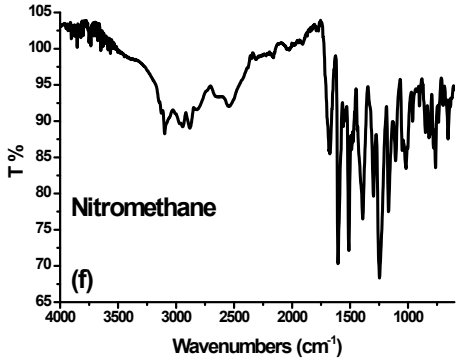
Nitromethane
(f)
T %
Wavenumbers (cm-1)

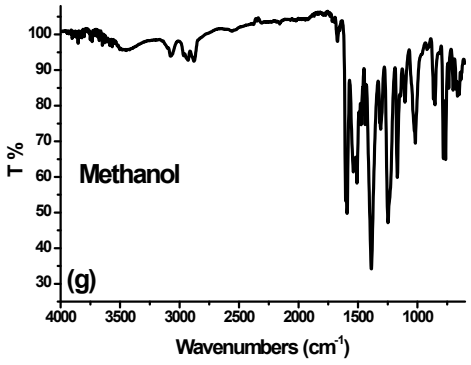
Methanol
(g)
T %
Wavenumbers (cm-1)

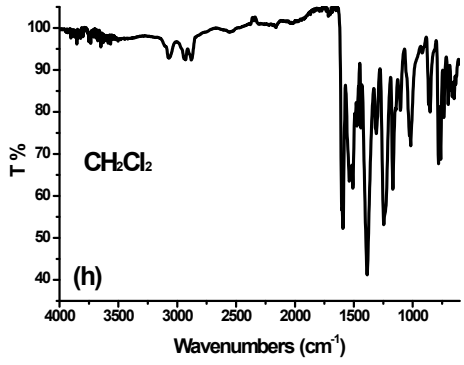
CH2Cl2
(h)
T %
Wavenumbers (cm-1)

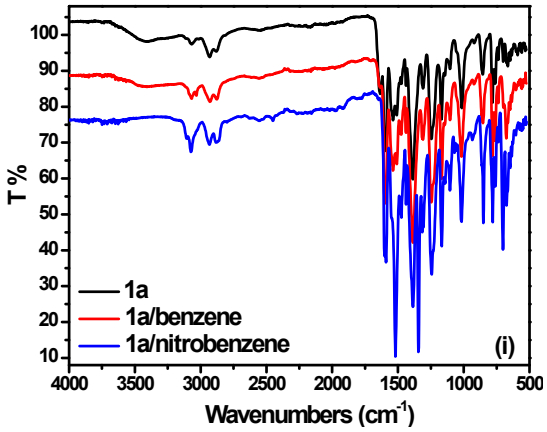
1a
1a/benzene
1a/nitrobenzene
(i)
T %
Wavenumbers (cm-1)

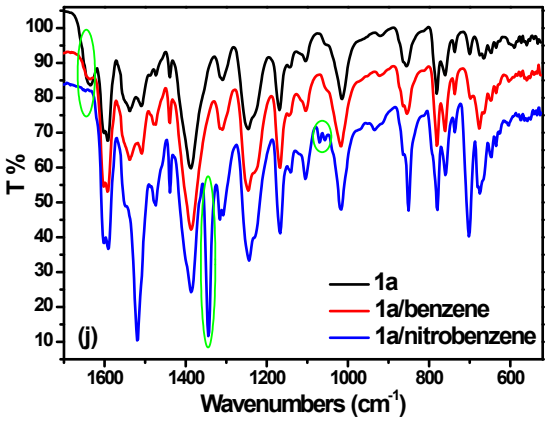
1a
1a/benzene
1a/nitrobenzene
(j)
T %
Wavenumbers (cm-1)

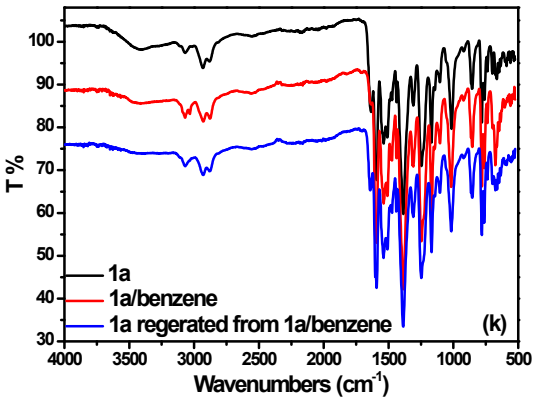
1a
1a/benzene
1a regerated from 1a/benzene
(k)
T %
Wavenumbers (cm-1)

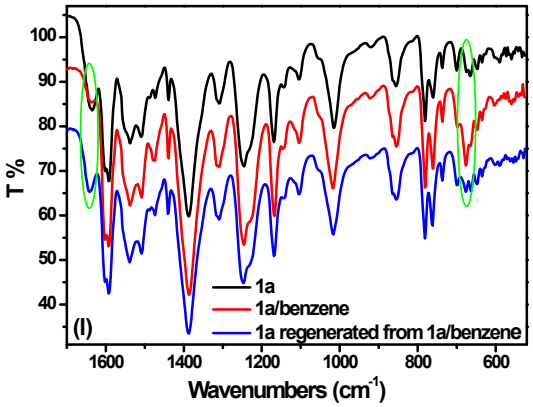
1a
1a/benzene
1a regenerated from 1a/benzene
(l)
T %
Wavenumbers (cm-1)

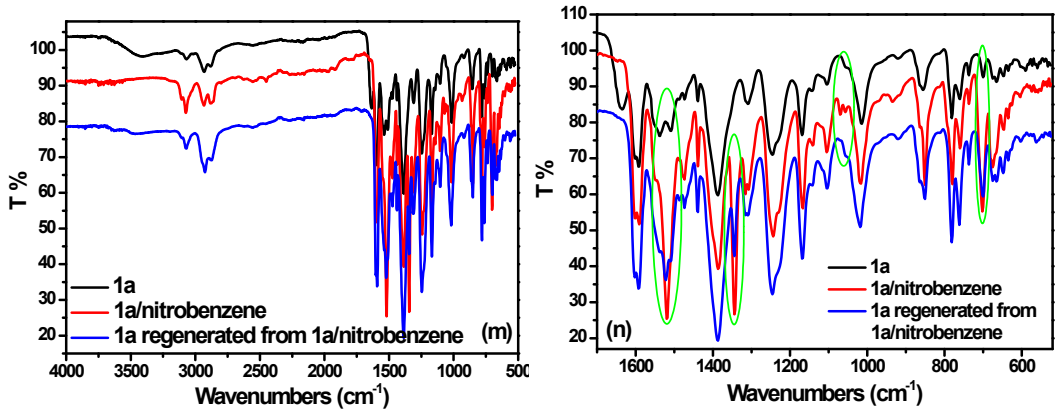

Fig. S10 IR spectra of solvent-soaked Cd-MOF (**1**) (a-h); the contrastive spectra of **1a**, **1a**/benzene, and **1a**/nitrobenzene (i) as well as the related partial enlarged drawing (j); the contrastive spectra of **1a**, **1a**/benzene and **1a** regenerated from 1a/benzene (k), as well as **1a**, **1a**/nitrobenzene and **1a** regenerated from **1a**/nitrobenzene (m), and the corresponding enlarged drawing (l and n).

4. Luminescence studies

The solid luminescence spectra of ligands (bipy and H_6L), and Cd-MOF (**1**) at room temperature are shown in Fig. S11. Free bipy ligand displays two main fluorescent emission bands at λ_{max} = 392 and 411 nm under excitation at 363 nm, which can be assigned to $\pi^* \rightarrow \pi$ transitions. When excited with λ_{ex}= 348 nm, free carboxylate ligand (H_6L) gives two strong sharp peaks at 382 and 401 nm, and one weak shoulder peak at 423 nm, due to the intraligand and ligand-to-ligand charge transition. Cd-MOF (**1**) exhibits a strong broad emission band locating at around 427 nm upon excitation at 324 nm, in which the coefficient of carboxylate and bipy ligands with metal centers contributes to the fluorescent emission.

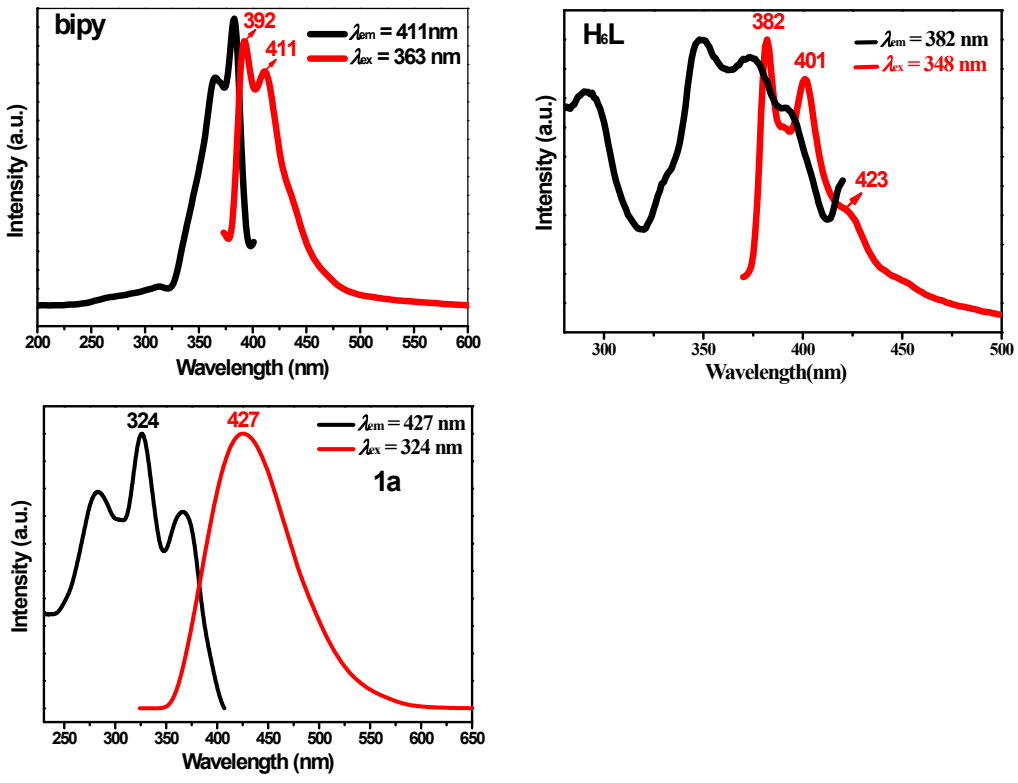

Fig. S11 Solid state excitation and emission spectra of free bipy and H_6L ligands, as well as Cd-MOF (**1**) at room temperature.

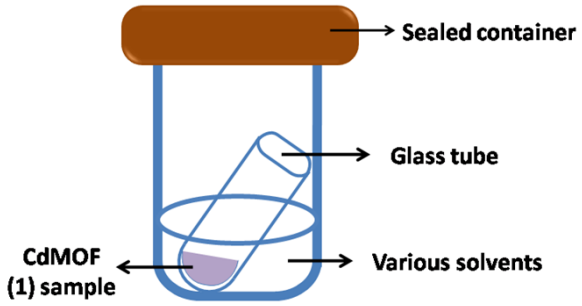

Fig. S12 Diagram of gas-sensing measurements for various solvent vapors. This experiment is executed similar to previous procedures described in *Angew.Chem. Int. Ed.* **2013**, *52*, 710; *Chem. Eur. J.* **2013**, *19*, 17172; *Chem. Commun.* **2014**, *50*, 10506.

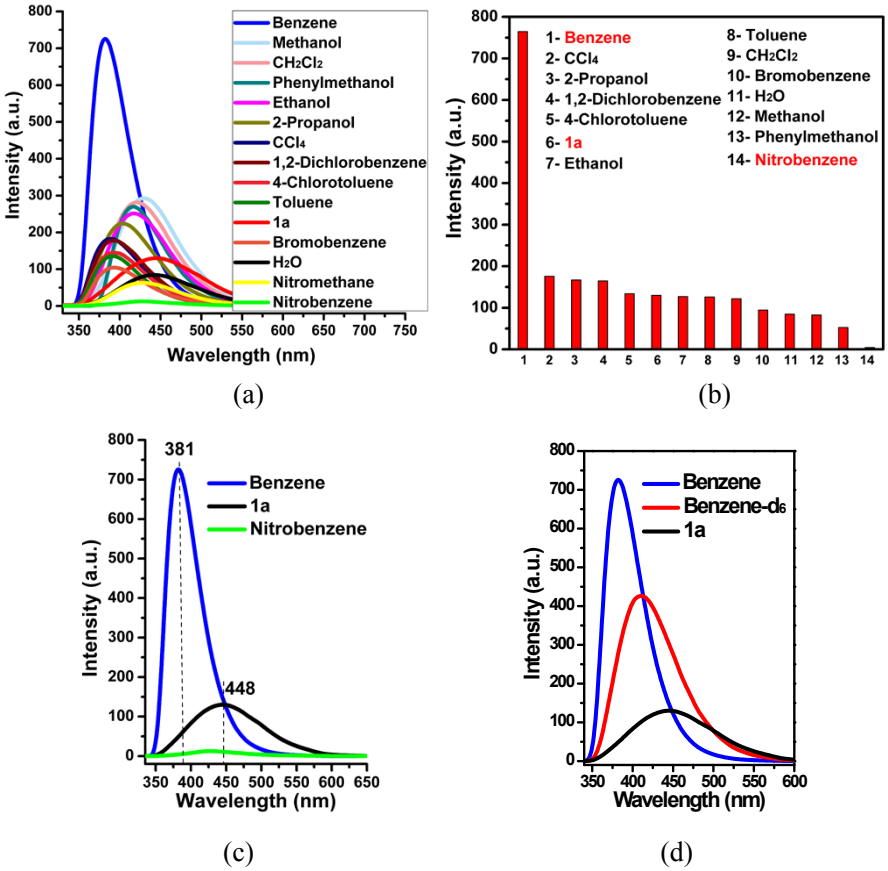

Fig. S13 (a) The luminescence spectra of **1a** after exposure to solvent vapors for 24h when excited at 314 nm. (b) The comparison diagram between **1a**, **1a**/benzene and **1a**/nitrobenzene. (c) The related luminescent intensity of **1a** at 381 nm. (d) The luminescence spectra of **1a**, **1a**/benzene, and **1a**/benzene-d_6 (C_6D_6).

The fluorescence properties of **1a** were investigated in various solvent emulsions at room temperature. The **1a**-solvent emulsions were prepared by introducing **1a** (5.0 mg) as a powder into various solvents (each 3.0 mL), treated with ultrasonication, and then aged to form stable

emulsions prior to fluorescence measurements.

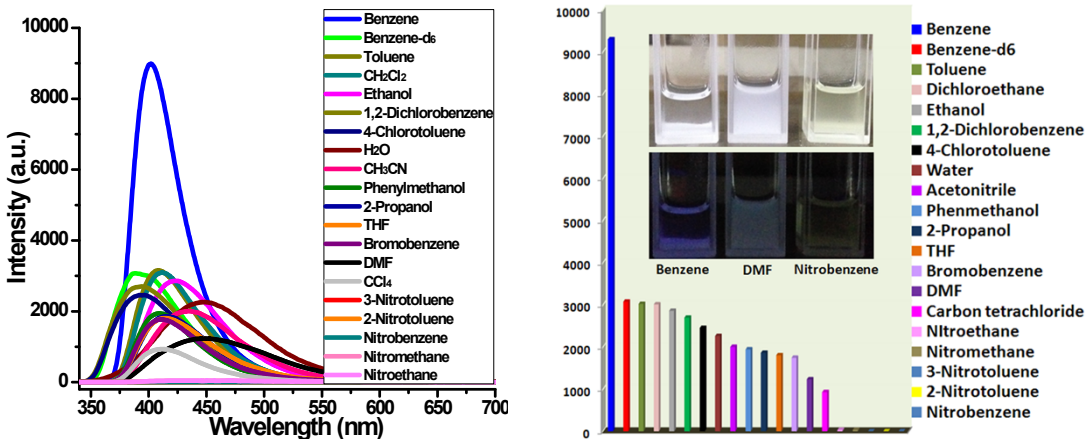

(a) (b)

Fig. S14 PL spectra (a) (λ_{ex} = 314 nm) and luminescence intensity at the maximum (b) of **1a** introduced into various pure solvents.

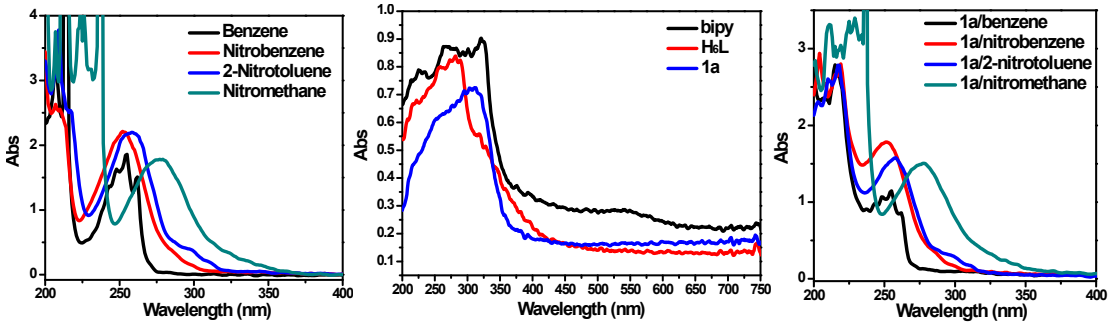

(a) (b) (c)

Fig. S15 (a) Absorption spectra of target solvents (benzene, nitrobenzene, 2-nitrotoluene, and nitromethane) in *n*-hexane. (b) The solid state absorption spectra of free ligands (H_6L, and bipy), and Cd-MOF (**1**). (c) Absorption spectra of **1a**-solvent emulsions in benzene (**1a/benzene**), nitrobenzene (**1a/nitrobenzene**), 2-nitrotoluene (**1a/2-nitrotoluene**), and nitromethane (**1a/nitromethane**).

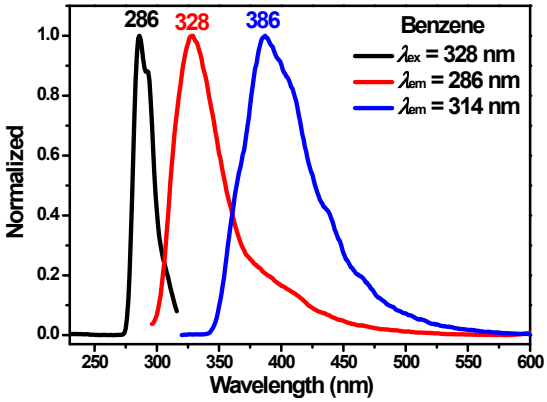

Fig. S16 The PL spectra of pure benzene solution.

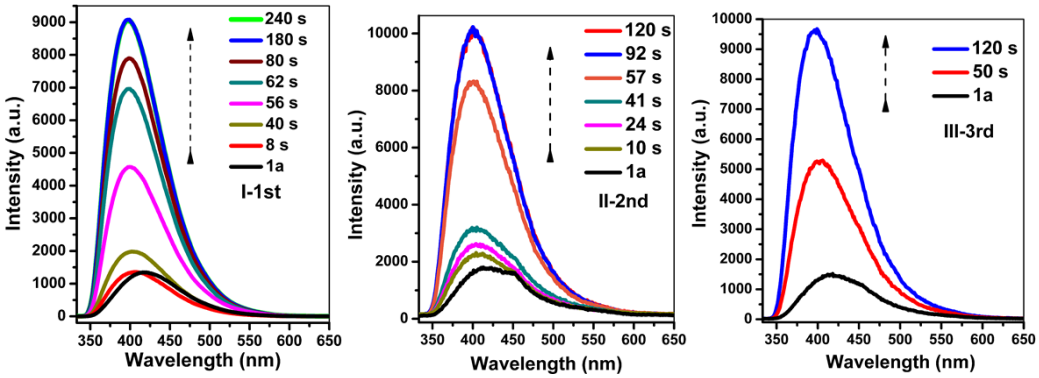

Fig. S17 Emission spectra of **1a** upon exposure to benzene vapor at various time intervals at room temperature. Reproducibility of the enhancing ability of **1a** to benzene vapor, the 1st cycle, 2nd cycle, and 3rd cycle, respectively.

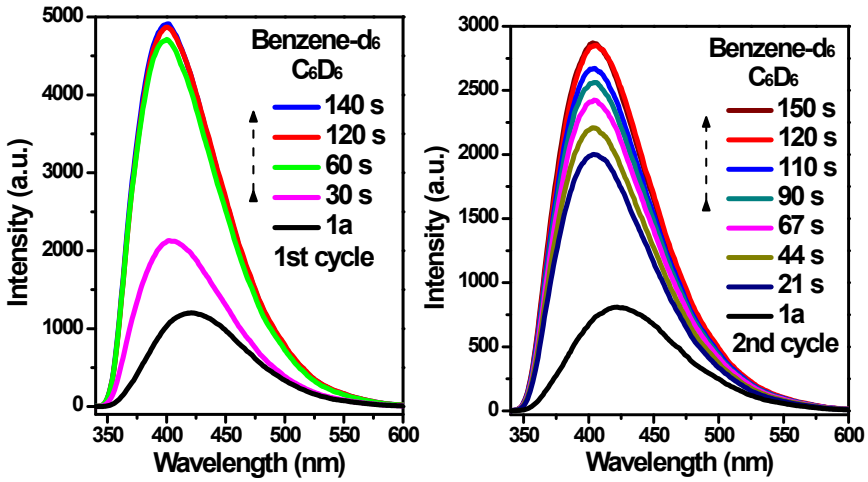

Fig. S18 Emission spectra of **1a** upon exposure to benzene-d_6 (C_6D_6) vapor at various time intervals at room temperature. Reproducibility of the enhancing ability of **1a** to **C_6D_6** vapor, the 1st cycle, and 2nd cycle respectively.

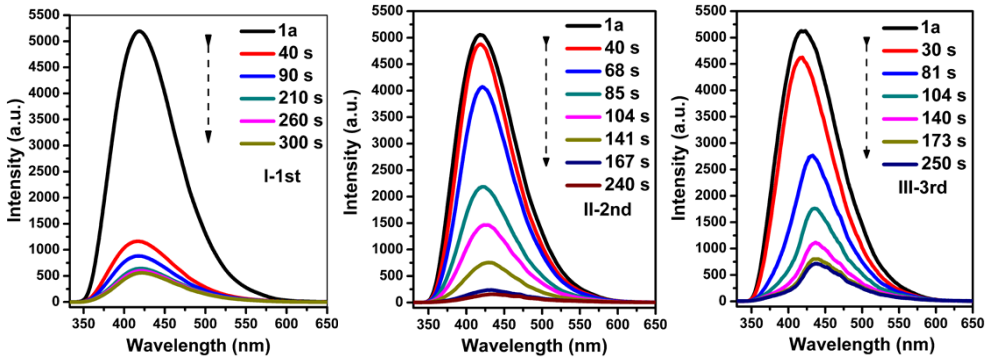

Fig. S19 Emission spectra of **1a** upon exposure to nitrobenzene vapor at various time intervals at room temperature. Reproducibility of the enhancing ability of **1a** to nitrobenzene vapor was carried for three cycles, namely, I-1st, II-2nd, III-3rd.

In order to test that the used powder of **1a** after detection of benzene vapor is reused and fully reversible, the used powder was heating at 80 °C for 3 hour under vacuum, then repeated this sensing experiment for three cycles. The results (Fig. S17) show the turn-on photoluminescent

effect for **1a** can be recovered without notable loss of the sensibility. The powder of **1a** was used for sensing of nitrobenzene vapor is also similar and reusable (Fig. S19).

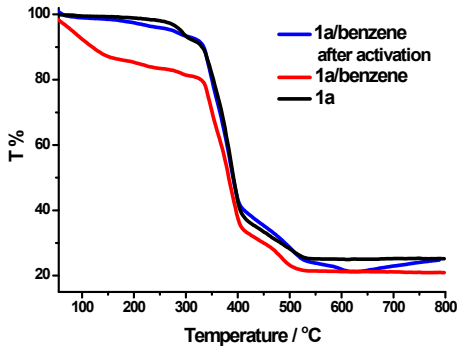

Fig. S20 TGA curves of **1a**, **1a/benzene**, and **1a/benzene after activation under vacuum**.

TGA curve of **1a** after immersing benzene (Fig. S20-red) shows that the weight loss of ~20% from 50 to 250 °C is observed, which is attributed to the loss of the exchanged benzene molecules in channel. In fact, the weight loss of benzene adsorbed in the surface has begun from room temperature, so the amount of trapping benzene molecules by the framework of **1a** is much more than 20%, which are stably trapped inside the channel. As shown in Fig. S20-blue curve, **1a** after capturing benzene (**1a/benzene**) can be recovered by simply heating at 80 °C under vacuum for 3h.

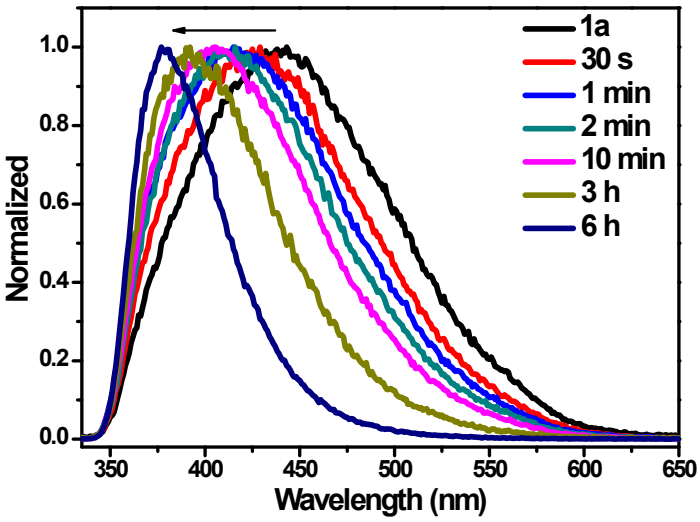

Fig. S21 The blue-shift of wavelength position for **1a** in benzene vapor at different time interval.

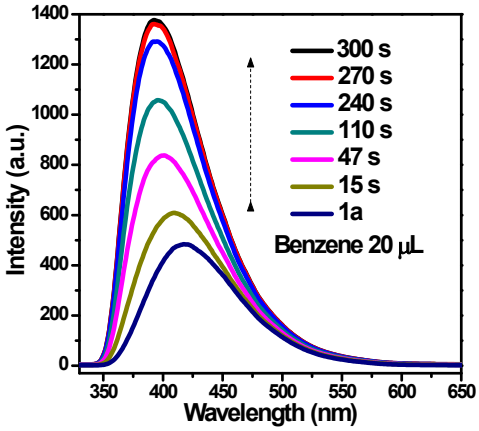

Fig.22 Emission spectra of **1a** upon exposure to benzene vapor with a low concentration of 8.8 mg/cm^3 at various time intervals at room temperature

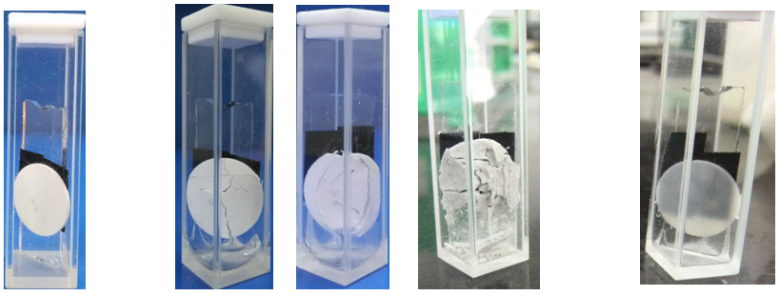

Fig. S23 The contrastive images of firm sheets before (a) in-situ solid state luminescent measurements, and after benzene vapors (b-d) as well as nitrobenzene vapors (e).

References:

1 (a) H.-Y. Wu, R.-X. Wang, W. Yang, J. Chen, Z.-M. Sun, J. Li and H. Zhang, *Inorg. Chem*. 2012, **51**, 3103; (b) F.-Y. Yi, J. Zhang, H.-X. Zhang and Z.-M. Sun, *Chem. Commun.*, 2012, **48**, 10419; (c) F.-Y. Yi, W. Yang and Z.-M. Sun, *J. Mater. Chem.*, 2012, **22**, 23201; (d) E. M. D. Keegstra, J. W. Zwikker, M. R. Roest and L. W. Jenneskens, *J. Org. Chem.*, 1992, **57**, 6678; (e) Y. -W. Wang, Y. -L. Zhang, W. Dou, A. -J. Zhang, W. -W. Qin and W. -S. Liu, *Dalton Trans.*, 2010, **39**, 9013; (f) D. Laliberte, T. Maris, A. Sirois and J. D. Wuest, *Org. Lett.*, 2003, **5**, 4787; (g) D. Laliberte, T. Maris and J. D. Wuest, *J. Org. Chem.*, 2004, **69**, 1776; (f) J. Cho, T. Keith Hollis, E. J. Valente and J. M. Trate, *J. Organomet. Chem.*, 2011, **696**, 373.

2 M. J. Frisch, G. W. Trucks, H. B. Schlegel, G. E. Scuseria, M. A. Robb, J. R. Cheeseman, G. Scalmani, V. Barone, B. Mennucci, G. A. Petersson, H. Nakatsuji, M. Caricato, X. Li, H. P. Hratchian, A. F. Izmaylov, J. Bloino, G. Zheng, J. L. Sonnenberg, M. Hada, M. Ehara, K. Toyota, R. Fukuda, J. Hasegawa, M. Ishida, T. Nakajima, Y. Honda, O. Kitao, H. Nakai, T. Vreven, J. A. Montgomery Jr., J. E. Peralta, F. Ogliaro, M. Bearpark, J. J. Heyd, E. Brothers, K. N. Kudin, V. N. Staroverov, T. Keith, R. Kobayashi, J. Normand, K. Raghavachari, A. Rendell, J. C. Burant, S. S. Iyengar, J. Tomasi, M. Cossi, N. Rega, J. M. Millam, M. Klene, J.

E. Knox, J. B. Cross, V. Bakken, C. Adamo, J. Jaramillo, R. Gomperts, R. E. Stratmann, O. Yazyev, A. J. Austin, R. Cammi, C. Pomelli, J. W. Ochterski, R. L. Martin, K. Morokuma, V. G. Zakrzewski, G. A. Voth, P. Salvador, J. J. Dannenberg, S. Dapprich, A. D. Daniels, O. Farkas, J. B. Foresman, J. V. Ortiz, J. Cioslowski and D. J. Fox, *GAUSSIAN 09 (Revision B.01)*, Gaussian, Inc., Wallingford, CT, 2010.

3. (a) A. D. Becke, *Phys. Rev. A*, 1988, **38**, 3098; (b) C. Lee, W. Yang and R. G. Parr, *Phys. Rev. B: Condens. Matter*, 1988, **37**, 785; (c) Y. Si, Y. Liu, X. Qu, Y. Wang and Z. Wu, *Dalton Trans.* 2013, **42**, 14149.
4. J. Autschbach, T. Ziegler, S. J. A. Gisbergen and E. J. Baerends, *J. Chem. Phys.* 2002, **116**, 6930.
5. T. Helgaker and P. Jørgemsen, *J. Chem. Phys.*, 1991, **95**, 2595.
6. K. L. Bak, P. Jørgemsen, T. Hel-gaker, K. Rund and H. J. A. Jensen, *J. Chem. Phys.*, 1993, **98**, 8873.
7. E. Cancès, B. Mennucci and J. Tomasi, *J. Chem. Phys.*, 1997, **107**, 3032.
8. M. Cossi, V. Barone, B. Mennucci and J. Tomasi, *Chem. Phys. Lett.*, 1998, **286**, 253.
9. B. Mennucci and J. Tomasi, *J. Chem. Phys.*, 1997, **106**, 5151.
10. N. M. O'Boyle, A. L. Tenderholt and K. M. Langner, *J. Comput. Chem.*, 2008, **29**, 839.
11. G. M. Sheldrick, SADABS; University of Göttingen: Germany, 1996.
12. (a) G. M. Sheldrick, *SHELXS-97*, Program for X-ray Crystal Structure Determination; University of Gottingen: Germany, 1997; (b) G. M. Sheldrick, *SHELXL-97*, Program for X-ray Crystal Structure Refinement; University of Gottingen: Germany, 1997; (c) CrystalClear, version 1.3.5; Rigaku Corp.: Woodlands, TX, 1999; (d) G. M. Sheldrick, *SHELX-96*: Program for Crystal Structure Determination; Siemens Analytical X-ray Instruments: Madison, WI, 1996.